

New Magic Numbers in $Ti_xC_y^-$ Anion Clusters and Implications for the Growth Mechanisms of Titanium Carbide Clusters

Lai-Sheng Wang,^{*,†,‡} Xue-Bin Wang,[‡] Hongbin Wu,[‡] and Hansong Cheng^{*,§}

Contribution from the Department of Physics, Washington State University, Richland, Washington 99352, Environmental Molecular Sciences Laboratory, Pacific Northwest National Laboratory, MS K8-88, P.O. Box 999, Richland, Washington 99352, and Air Products and Chemicals, Inc., 7201 Hamilton Boulevard, Allentown, Pennsylvania 18195

Received December 11, 1997

Abstract: We report observation of new prominent peaks in the $Ti_xC_y^-$ anion mass spectra from laser vaporization experiments involving a pure Ti target with a CH_4 -seeded He carrier gas. Both photoelectron spectroscopy and density functional calculations were performed to obtain structural and bonding information for the new prominent anion clusters, including $Ti_3C_8^-$, $Ti_4C_8^-$, $Ti_6C_{13}^-$, $Ti_7C_{13}^-$, $Ti_9C_{15}^-$, and $Ti_{13}C_{22}^-$. For each cluster, we optimized several structures, evaluated their electron affinities (EAs), and simulated their single particle density of states (DOS). The calculated EAs and DOS of the different structures were then compared with the experimental photoelectron data. Good agreement between the experiments and calculations was found for the lowest energy isomers considered in each case. We found that three factors, i.e., the C_2 dimer, cubic framework, and layered structures, play essential roles in determining the structures and chemical bonding of the titanium carbide clusters. A growth pathway from Ti_3C_8 to $Ti_{13}C_{22}$ with Ti_6C_{13} , Ti_7C_{13} , and Ti_9C_{15} as intermediates is proposed and discussed.

Introduction

Metallo-carbohedrenes (MetCar) containing 8 early transition metal atoms and 12 C atoms were discovered in 1992 by Castleman and co-workers and were proposed as a new class of stable molecular clusters.¹ The MetCars were observed as abundant (magic) *positive* ion peaks in mass spectra from laser vaporization experiments of the pure metals with hydrocarbon-seeded carrier gases.^{1,2} A dodecahedral structure of T_h point group symmetry, a cage-like molecular shape similar to fullerenes, was proposed to account for the apparent stability of these magic clusters. However, the definitive structures and growth mechanisms of the MetCars are still lacking, despite extensive theoretical^{3–5} and experimental efforts.^{6–9}

Unlike the fullerenes, which grow by expanding the cage, Wei et al. proposed that the MetCars follow a multicage growth path, based on their observation of magic cluster cations in mass spectra of zirconium carbide clusters at $Zr_{13}C_{22}^+$, $Zr_{18}C_{29}^+$, and $Zr_{22}C_{35}^+$.¹⁰ However, Pilgrim and Duncan subsequently showed that Ti and V carbide clusters form cubic nanocrystals with a composition of $M_{14}C_{13}^+$, a $3 \times 3 \times 3$ cubic cluster much like the bulk crystal lattice.¹¹ The composition for the double-cage at $M_{13}C_{22}^+$ was not observed. To explain these paradoxical observations, Reddy and Khanna suggested that the formation of multicage MetCars or cubic structures depends on the Ti/C ratios: low Ti/C ratio favors MetCar formation due to abundant C_2 dimers.¹² Wei et al. provided evidence in the Nb carbide

[†] Alfred P. Sloan Research Fellow.

[‡] Washington State University and Pacific Northwest National Laboratory.

[§] Air Products and Chemicals, Inc.

(1) Guo, B. C.; Kerns, K. P.; Castleman, A. W., Jr. *Science* **1992**, *255*, 1411. Guo, B. C.; Wei, S.; Purnell, J.; Buzza, S.; Castleman, A. W., Jr. *Science* **1992**, *256*, 511.

(2) Pilgrim, J. S.; Duncan, M. A. *J. Am. Chem. Soc.* **1993**, *115*, 6958.

(3) Grimes, R. W.; Gale, J. D. *J. Chem. Soc., Chem. Commun.* **1992**, 1222. Rantala, T. T.; Jelski, D. A.; Bowser, J. R.; Xia, X.; George, T. F. *Z. Phys. D* **1992**, *26*, S255. Pauling, L. *Proc. Natl. Acad. Sci. U.S.A.* **1992**, *89*, 8175. Lin, Z.; Hall, M. B. *J. Am. Chem. Soc.* **1992**, *114*, 10054. Reddy, B. V.; Khanna, S. N.; Jena, P. *Science* **1992**, *258*, 640. Methfessel, M.; van Schilfgaarde, M.; Scheffler, M. *Phys. Rev. Lett.* **1993**, *71*, 209. Hay, P. J. *J. Phys. Chem.* **1993**, *97*, 3081. Grimes, R. W.; Gale, J. D. *J. Phys. Chem.* **1993**, *97*, 4616; Khan, A. *J. Phys. Chem.* **1995**, *99*, 4923. Lou, L.; Guo, T.; Nordlander, P.; Smalley, R. E. *J. Chem. Phys.* **1993**, *99*, 5301.

(4) Ceulemans, A.; Fowler, P. W. *J. Chem. Soc., Faraday Trans.* **1992**, *88*, 2797. Rohmer, M.; de Vaal, P.; Benard, M. *J. Am. Chem. Soc.* **1992**, *114*, 9696. Chen, H.; Feyerhergen, M.; Long, X. P.; Fitzgerald, G. *Phys. Rev. Lett.* **1993**, *71*, 1732.

(5) Dance, D. *J. Chem. Soc., Chem. Commun.* **1992**, 1779. Rohmer, M.; Benard, M.; Henriot, C.; Bo, C.; Poblet, J. *J. Chem. Soc., Chem. Commun.* **1993**, 1182. Dance, I. *J. Am. Chem. Soc.* **1996**, *118*, 2699, 6309. Lin, Z.; Hall, M. B. *J. Am. Chem. Soc.* **1993**, *115*, 11165. Rohmer, M.; Benard, M.; Bo, C.; Poblet, J. *J. Am. Chem. Soc.* **1995**, *117*, 508. Rohmer, M.; Benard, M.; Bo, C.; Poblet, J. *J. Phys. Chem.* **1995**, *99*, 16913.

(6) Wei, S.; Guo, B. C.; Purnell, J.; Buzza, S.; Castleman, A. W., Jr. *J. Phys. Chem.* **1992**, *96*, 4166. May, B. D.; Cartier, S. F.; Castleman, A. W., Jr. *Chem. Phys. Lett.* **1995**, *242*, 265. Cartier, S. F.; May, B. D.; Castleman, A. W., Jr. *Chem. Phys. Lett.* **1994**, *116*, 5295. Cartier, S. F.; May, B. D.; Castleman, A. W., Jr. *J. Chem. Phys.* **1994**, *100*, 5384. Kerns, K. P.; Guo, B. C.; Deng, H. T.; Castleman, A. W., Jr. *J. Chem. Phys.* **1994**, *101*, 8529. Cartier, S. F.; May, B. D.; Castleman, A. W., Jr. *J. Chem. Phys.* **1996**, *104*, 3423. Cartier, S. F.; May, B. D.; Castleman, A. W., Jr. *J. Phys. Chem.* **1996**, *100*, 8175. Kerns, K. P.; Guo, B. C.; Deng, H. T.; Castleman, A. W., Jr. *J. Am. Chem. Soc.* **1995**, *117*, 4026. Deng, H. T.; Kerns, K. P.; Castleman, A. W., Jr. *J. Am. Chem. Soc.* **1996**, *118*, 446.

(7) Pilgrim, J. S.; Duncan, M. A. *J. Am. Chem. Soc.* **1993**, *115*, 4395. Pilgrim, J. S.; Brock, L. R.; Duncan, M. A. *J. Phys. Chem.* **1995**, *99*, 544. Brock, L. R.; Duncan, M. A. *J. Phys. Chem.* **1996**, *100*, 5654.

(8) Byun, Y. G.; Lee, S. A.; Freiser, B. S. *J. Phys. Chem.* **1996**, *100*, 14281. Yeh, C. S.; Afzaal, S.; Lee, S. A.; Byun, Y. G.; Freiser, B. S. *J. Am. Chem. Soc.* **1994**, *116*, 8806. Byun, Y. G.; Freiser, B. S. *J. Phys. Chem.* **1996**, *118*, 3681.

(9) Lee, S.; Gotts, N. G.; von Helden, G.; Bowers, M. T. *Science* **1995**, *267*, 999.

(10) Wei, S.; Guo, B. C.; Purnell, J.; Buzza, S.; Castleman, A. W., Jr. *Science* **1992**, *256*, 818.

(11) Pilgrim, J. S.; Duncan, M. A. *J. Am. Chem. Soc.* **1993**, *115*, 9724. Pilgrim, J. S.; Duncan, M. A. *Int. J. Mass Spectrom. Ion Processes* **1994**, *138*, 283.

(12) Reddy, B. V.; Khanna, S. N. *Chem. Phys. Lett.* **1993**, *209*, 104. Reddy, B. V.; Khanna, S. N. *J. Phys. Chem.* **1994**, *98*, 9446.

system, showing that the MetCars or nanocrystals can be formed at different experimental conditions.¹³ However, all these studies were done with the positive ions. There has been little work focused on the anions that are produced at the same time during the plasma reactions in the laser vaporization cluster source.

We have been interested in the electronic structure and formation mechanisms of the MetCars.^{14–16} In a very recent work, we combined anion photoelectron spectroscopy (PES) and density functional theory (DFT) calculations to elucidate the structure of the $Ti_{13}C_{22}$ cluster.¹⁵ We found that $Ti_{13}C_{22}$ has an unusual cubic structure with 8 C_2 dimers at the cube corners. This observation led to the proposal of a novel layer-by-layer growth model for the large carbide clusters that can account uniquely for the magic numbers in the multicage growth model.

Even though the $Ti_8C_{12}^-$ anion was not produced in laser vaporization of a pure Ti target in a CH_4 -seeded He carrier gas,^{14–16} there are other magic peaks in the negative ion mass spectrum of $Ti_xC_y^-$, occurring at $x/y = 3/8, 4/8, 6/13, 7/13,$ and $9/15$. In the current work, we present our detailed studies on the structure and bonding of these smaller magic numbers and the implication to the growth pathways of the metal carbide clusters. We have obtained PES spectra of all these clusters and further performed DFT calculations. The calculated electron affinities (EAs) and single particle density of states (DOS) were compared with the experimental measurements. Structural information was obtained from the combined experimental and theoretical studies and was used to understand the growth pathways of the carbide clusters.

Experimental and Computational Methods

The experimental apparatus used in this study consists of a laser vaporization cluster source, a time-of-flight (TOF) mass spectrometer, and a magnetic-bottle PES analyzer. The details of our apparatus and experimental procedures have been published before.^{17,18} Briefly, a pure Ti target was vaporized with a 10–15 mJ laser pulse from a Nd:YAG laser (532 nm). The laser-produced plasma was mixed with a helium carrier gas containing 5% CH_4 (10 atm stagnation pressure). The plasma reactions between Ti and the hydrocarbon produced a series of Ti_xC_y clusters in both neutral and charged states. The clusters, entrained in the carrier gas, expanded through a 2 mm diameter nozzle to form a supersonic cluster beam. The anions were extracted at 90° into the TOF mass spectrometer for size analyses. Mass spectra of the anions were usually taken by averaging 1000 vaporization laser shots. For the PES experiments, a cluster of interest was selected by a mass gate and decelerated before photodetachment by an ArF excimer laser (193 nm) or a Nd:YAG laser (266 and 355 nm). The PES experiments were performed at 20 Hz repetition rate with the vaporization laser off at alternating detachment laser shots for background subtraction at 266 and 193 nm. The measured photoelectron TOF spectra were calibrated with the known spectra of Cu^- to obtain the binding energy spectra usually presented. The resolution of our apparatus is better than 30 meV for 1 eV electrons and deteriorates for high energy electrons often encountered at 193 nm.

The theoretical calculations were performed with a gradient-corrected DFT method. Full geometry optimization was carried out for all the

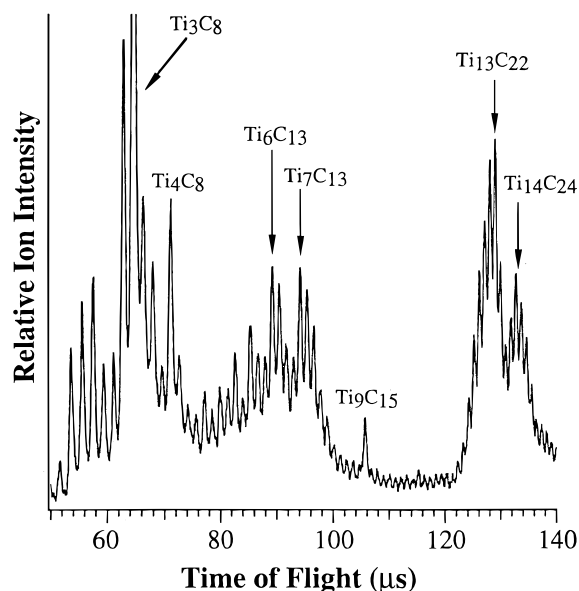


Figure 1. Mass spectra of $Ti_xC_y^-$ anions from laser vaporization of a pure Ti target with a He carrier gas containing 5% CH_4 . Note the $Ti_3C_8^-$ peak is out of scale and is twice the full scale.

cluster structures. The DFT calculations employed Becke's gradient-corrected exchange functional¹⁹ and Perdew–Wang's gradient-corrected correlation functional.²⁰ The gradient correction was incorporated in the SCF cycles iteratively. A double numerical basis set augmented with polarization functions was used and all inner core electrons were frozen. The spin polarized Kohn–Sham scheme was utilized, yielding exclusively closed-shell electronic structures for all the clusters. Very similar results were also obtained when a spin-restricted scheme was adopted. All of the results discussed in this article were obtained from the spin-polarized calculations with DMol.²¹ We optimized structures of both the anions and neutrals. The energy differences between the anions and the respective neutrals gave the adiabatic EAs. The DOS spectra of the anions were simulated by convoluting Gaussians to occupied single particle energy levels and used to compare qualitatively to the observed PES spectra.

Results and Discussion

Anion Cluster Distribution: New Magic Numbers. Figure 1 shows a mass spectrum of $Ti_xC_y^-$ clusters, produced by laser vaporization of a Ti target with a 5% CH_4/He carrier gas. The anion spectrum differs significantly from the positive ion mass spectra, where the $Ti_8C_{12}^+$ MetCar peak and the $Ti_{14}C_{13}^+$ cubic cluster dominate the low and higher mass range, respectively.^{1,2} Several prominent anion clusters are observed, namely, $Ti_3C_8^-$, $Ti_4C_8^-$, $Ti_6C_{13}^-$, $Ti_7C_{13}^-$, $Ti_9C_{15}^-$, and $Ti_{13}C_{22}^-$. The exact compositions of the labeled peaks were confirmed by using ^{13}C isotope-substituted CH_4 seeded in He; the mass degeneracy between one Ti and four C was broken in the ^{13}C case, as shown clearly in Figure 2. Most surprising in the anion mass distribution is the total absence of the anticipated Ti_8C_{12} peak, which is so prominent in the positive ion channel. The mass peaks beyond 7/13 in Figure 2 are equally spaced by one ^{13}C ; the 8/12 MetCar is degenerate with the 7/16 cluster in the ^{12}C case (Figure 1) and should show up to the left of the 7/16 peak in the ^{13}C case (Figure 2). The anion mass spectrum, in fact, shows that clusters containing 8 to 12 Ti atoms, between 100 and 120 μs in Figure 1, have very low abundance, except $Ti_9C_{15}^-$, which shows up as a prominent peak in an otherwise

(13) Wei, S.; Guo, B. C.; Deng, H. T.; Purnell, J.; Buzza, S.; Castleman, A. W., Jr. *J. Am. Chem. Soc.* **1994**, *116*, 4475.

(14) Wang, L. S.; Li, S.; Wu, H. *J. Phys. Chem.* **1996**, *100*, 19211.

(15) Wang, L. S.; Cheng, H. S. *Phys. Rev. Lett.* **1997**, *78*, 2983.

(16) Li, S.; Wu, H.; Wang, L. S. *J. Am. Chem. Soc.* **1997**, *119*, 7417.

(17) Wang, L. S.; Cheng, H.; Fan, J. *J. Chem. Phys.* **1995**, *102*, 9480; Wu, H.; Desai, S. R.; Wang, L. S., *Phys. Rev. Lett.* **1996**, *76*, 212; Wa, H.; Desai, S. R.; Wang, L. S. *J. Phys. Chem.* **1997**, *101*, 2103.

(18) Wang, L. S.; Wu, H. Probing the Electronic Structure of Transition Metal Clusters From Molecular to Bulklike Using Photoelectron Spectroscopy. In *Advances in Metal and Semiconductor Clusters*; Duncan, M. A., Ed.; JAI Press: Greenwich, 1998; Vol. 4, p 299.

(19) Becke, A. D. *Phys. Rev. A* **1988**, *38*, 3098.

(20) Perdew, J. P.; Wang, Y. *Phys. Rev. B* **1992**, *45*, 13244.

(21) DMol 96.0, September 1996, San Diego, Molecular Simulations, 1996.

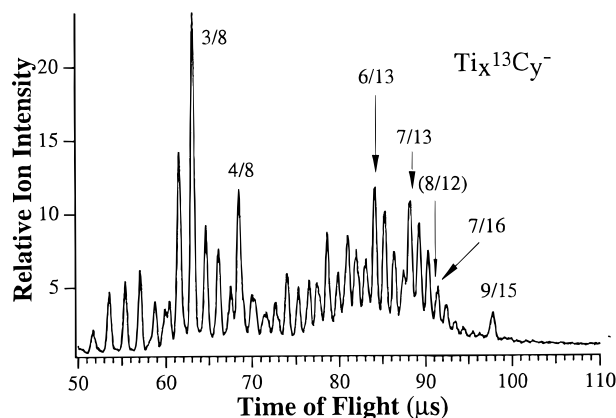


Figure 2. Mass spectra of Ti_xC_y^- anions using ^{13}C -substituted CH_4 . Note $\text{Ti}_8\text{C}_{12}^-$ is completely absent.

very low abundant mass range. The low abundance of the clusters containing 8 to 12 Ti atoms suggests that either these clusters are relatively unstable or the growth kinetics are such that they form the 13/22 cluster rapidly. In either case, the 9/15 cluster is unusually abundant and should provide clues for the growth from small clusters to the 13/22 cluster.

The $\text{Ti}_{13}\text{C}_{22}$ cluster has the same composition as the previously observed $\text{Zr}_{13}\text{C}_{22}^+$ and $\text{Nb}_{13}\text{C}_{22}^+$ positive clusters which were proposed to have the double-cage structure.¹⁰ Recently, we have investigated the structure of the $\text{Ti}_{13}\text{C}_{22}$ cluster by combining PES and theoretical calculations.¹⁵ We proposed that the $\text{Ti}_{13}\text{C}_{22}$ cluster has an unusual cubic structure with 8 C_2 dimers occupying the 8 cube corners rather than the previously proposed double-cage structure. We also suggested that the Ti_9C_{15} cluster was an intermediate in the formation of the cubic $\text{Ti}_{13}\text{C}_{22}$ structure. However, the small magic clusters were not investigated in detail.

PES Spectra of the Magic Clusters: Ti_xC_y^- ($x/y = 3/8, 4/8, 6/13, 7/13,$ and $9/15$). The properties of the new magic clusters observed in the anions may be studied by a variety of experimental techniques, including PES and ion mobility measurements.⁹ PES is particularly useful to probe the electronic structure of these clusters and allows the EAs and electronic density of states of the neutral clusters to be measured directly.^{14–18} For example, recently, we have obtained PES spectra of five MetCars, providing valuable electronic and spectroscopic information that can be used to verify further theoretical calculations.¹⁶ We have also obtained PES spectra of a variety of Ti_xC_y^- clusters.²² In the present work, we focus our discussion on the small magic Ti_xC_y^- anion clusters.

Figure 3 shows the PES spectra of Ti_3C_8^- , Ti_4C_8^- , $\text{Ti}_6\text{C}_{13}^-$, $\text{Ti}_7\text{C}_{13}^-$, and $\text{Ti}_9\text{C}_{15}^-$ measured at 6.42 eV (193 nm) photon energy. These spectra represent transitions from the ground state of the anions to the states of the neutrals. All the spectra exhibit broad features, suggesting that there are significant geometry changes between the anions and neutrals or high densities of low-lying states. We have also taken spectra at lower photon energies to improve the spectral resolution for the lower binding energy features, but no fine structures were further resolved, probably due to the high densities of electronic states accompanied by excitations of many vibrational modes in the detachment processes. The resolved spectral features were reproducible under different experimental conditions, such as different stagnation pressures or laser vaporization power, and identical spectra were obtained when ^{13}C -isotope labeled

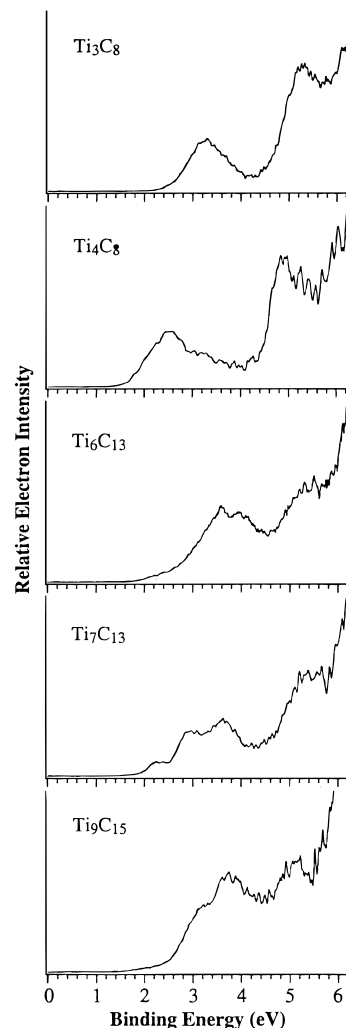


Figure 3. Photoelectron spectra of Ti_3C_8^- , Ti_4C_8^- , $\text{Ti}_6\text{C}_{13}^-$, $\text{Ti}_7\text{C}_{13}^-$, and $\text{Ti}_9\text{C}_{15}^-$ at 193 nm.

Table 1. Estimated Adiabatic Electron Affinities of the Ti_xC_y Clusters Compared to the Calculated Values (eV)^a

	Ti_3C_8	Ti_4C_8	Ti_6C_{13}	Ti_7C_{13}	Ti_9C_{15}
exptl ^a	2.5	1.8	2.2	2.1	1.8
calcd. (a) ^b	2.33	2.12	2.30	2.34	1.80
calcd. (b) ^c	2.65	0.84	2.97	2.88	2.05

^a The experimental uncertainties were estimated to be ± 0.2 eV due to the lack of sharp threshold features in the PES spectra. ^b Calculated electron affinity for isomer (a) in Figure 4. ^c Calculated electron affinity for isomer (b) in Figure 4.

CH_4 was used, suggesting that the observed spectra are mainly due to a single isomer or a consistent set of isomers. We also took PES spectra of Ti_3C_8^- and Ti_4C_8^- produced by using a TiC target with pure He carrier gas and obtained identical spectra.

From the detachment thresholds, EAs for the neutral clusters can be determined. If sharp features or 0–0 vibrational transitions can be clearly resolved, the adiabatic EAs can be determined rather accurately from the anion PES spectra. However, due to the broad spectral features, the EAs in the present cases can only be estimated and are listed in Table 1. The EAs for these clusters are all quite high, reflecting their high carbon contents. The EA of the $\text{Ti}_{13}\text{C}_{22}$ cluster was measured to be 3.0 eV in our previous work.¹⁵ The high EAs of these clusters are in sharp contrast to that of the MetCar Ti_8C_{12} cluster, which has a very low EA of 1.05 eV.¹⁴

(22) Wang, X. B.; Ding, C. F.; Wang, L. S. *J. Phys. Chem. A* **1997**, *101*, 7699.

Theoretical Modeling. The broad PES features and lack of vibrational information make it difficult to interpret the spectra shown in Figure 3 without theoretical modeling. To obtain detailed information about the structure and bonding of these clusters, we carried out extensive DFT calculations. As demonstrated for $Ti_{13}C_{22}$, DFT should work well for these carbide clusters.¹⁵ The measured EAs and PES spectra can be used to compare with the calculated EAs and DOS so that reliable theoretical structural and electronic information can be obtained.

There may exist many possible isomers of the Ti_xC_y clusters. Currently, there are no feasible theoretical techniques which can search for the global minimum for the clusters studied in this work, particularly due to the presence of large numbers of transition metals in the clusters. Therefore, some initial knowledge of the bonding and structural motifs of the titanium carbide clusters was essential for judiciously selecting initial structures for the theoretical calculations. From previous investigations of MetCars¹⁻⁹ and our own work on $Ti_{13}C_{22}$,¹⁵ two structural features were noted: (1) C_2 dimers play an important role in the carbon-rich clusters, and (2) the cubic structural motif as exemplified in the $3 \times 3 \times 3$ cubic $Ti_{14}C_{13}^+$ nanocrystal and the C_2 -decorated cubic $Ti_{13}C_{22}$ cluster. Hence, for Ti_3C_8 and Ti_4C_8 we considered various configurations involving 3 and 4 Ti atoms and 4 C_2 dimers. For Ti_6C_{13} , Ti_7C_{13} , and Ti_9C_{15} , we calculated different configurations involving cubic structural motifs and various C_2 dimers. We optimized structures of both the anions and neutrals.

Figure 4 displays two optimized structures for each neutral cluster, Ti_3C_8 , Ti_4C_8 , Ti_6C_{13} , Ti_7C_{13} , and Ti_9C_{15} , with the lower energy one (higher atomic binding energy) shown on the left. The calculated atomic binding energy (shown in parentheses) and key structural parameters are indicated in Figure 4. The two previously obtained cubic structures of $Ti_{13}C_{22}$ are also listed for comparison.¹⁵ The calculated EAs are shown in Table 1 together with the measured ones. Of the clusters shown in Figure 4, the calculated binding energies for the two isomers are relatively close. The calculated EAs of the two isomers are also within about 0.5 eV for all the clusters except Ti_4C_8 . Importantly, the lower energy structure in each case yielded an EA in better agreement with the experimental value, as shown in Table 1, indicating the sensitivity of the calculated EAs to structure. The optimized cluster structures exhibit significant bond relaxation from the anions to the neutrals, consistent with the observed broad PES features.

Cluster Structures and Bonding. The optimized structures (Figure 4) suggest that carbon dimers indeed play an important role in stabilizing the clusters. We found that in all cases the low-lying states of C_2 are actively involved in the chemical bonding. In particular, we found that there is a net electron transfer from Ti to C_2 . Consequently, C_2 in the Ti_xC_y clusters can be viewed as acetylene-like C_2 anions, isoelectronic with CO and CN^- . Such Ti- C_2 interactions were found in Ti_8C_{12} , which involves 6 C_2 dimers.³⁻⁵ Detailed insight into the chemical bonding in the Ti_xC_y clusters can be obtained by analyzing the calculated wave functions and comparing the calculated DOS with the PES spectra. Here we give detailed discussions on the electronic structures of Ti_3C_8 and Ti_4C_8 ; the larger Ti_xC_y clusters exhibit similar features to these two smaller clusters.

For Ti_3C_8 , we optimized two structures, both involving a trigonal bipyramid Ti_3C_2 with 3 C_2 dimers. Structure (a), with the 3 C_2 dimers on the same plane as the 3 Ti atoms, is significantly more stable than structure (b), in which the 3 C_2

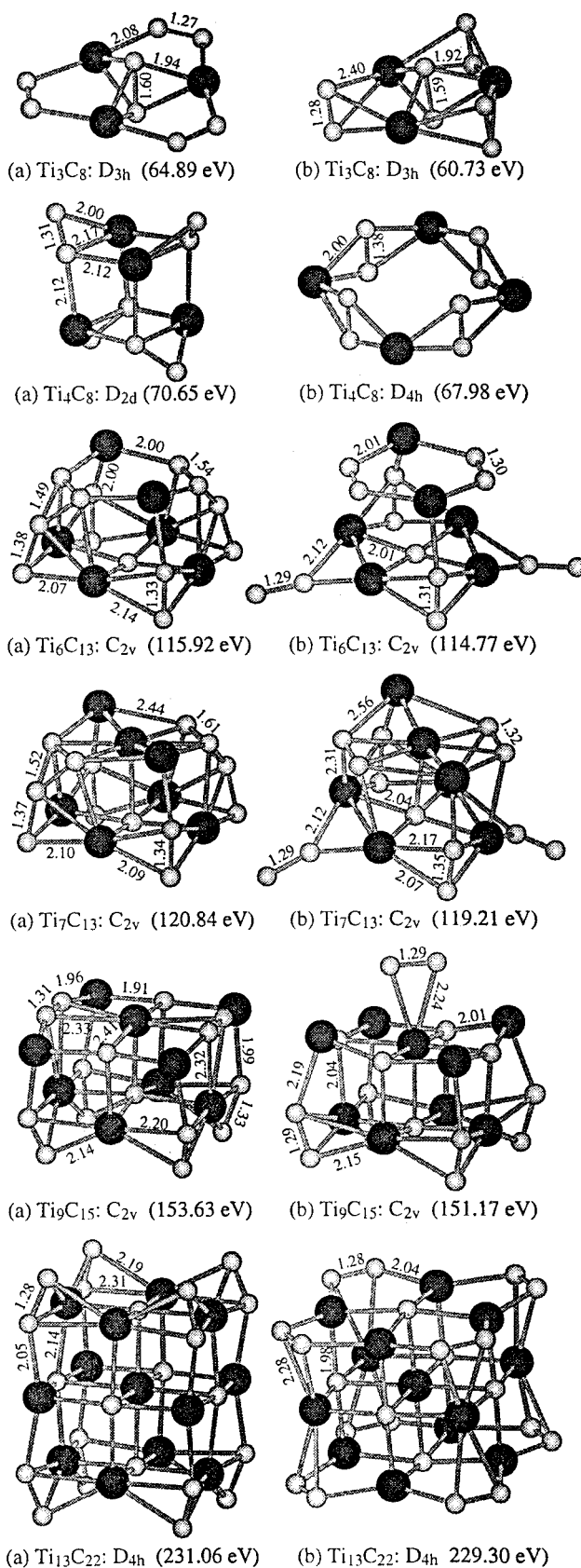
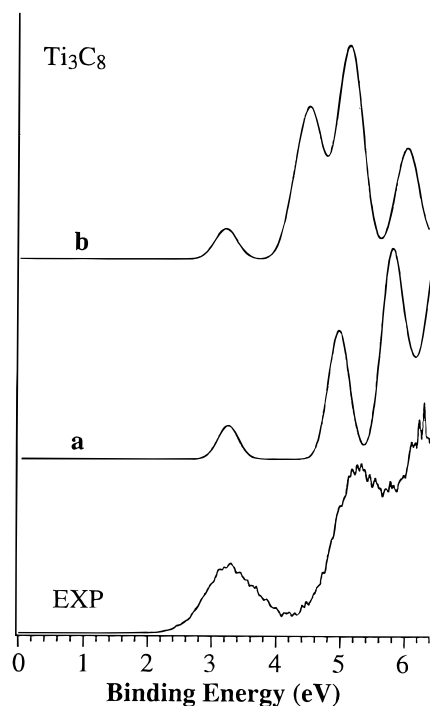


Figure 4. Optimized structures of the Ti_3C_8 , Ti_4C_8 , Ti_6C_{13} , Ti_7C_{13} , Ti_9C_{15} , and $Ti_{13}C_{22}$ clusters. The calculated atomic binding energies are also given in parentheses. Key bond distances shown are in Å.

dimers are vertical relative to the Ti_3 plane. The 3 C_2 dimers in both structures have very short C-C bond lengths, similar to a C-C triple bond whereby the distance between the two capping C atoms is considerably longer, facilitating the forma-

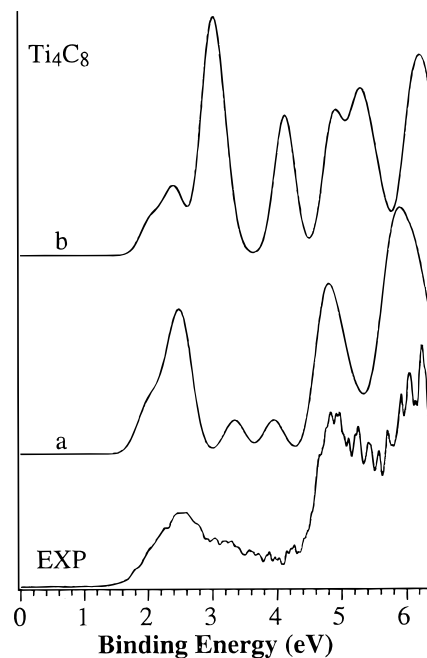
Table 2. Calculated Mulliken Charges on the Three C₂ Dimers, the Capping C Atoms, and the Ti Atoms in Ti₃C₈

structure	C ₂ dimers	capping C atom	Ti
a	-0.508	-0.662	+0.949
b	-0.580	-0.598	+0.979

**Figure 5.** Comparison of the photoelectron spectrum of Ti₃C₈⁻ to the calculated DOS of the two structures shown in Figure 4. The DOS is simulated by convoluting a 0.2 eV width Gaussian function onto the single particle occupied energy levels of the anions.

tion of more close-packed cluster structures. In structure (a), the bonding is primarily dominated by the nearly perfect orbital overlap between the π -orbitals of the 3 C₂ dimers and the well-oriented 3d-orbitals of Ti. In structure (b), however, the bonding is overwhelmingly dictated by the σ -orbitals of the C₂ dimers weakly mixed with the d_{z²}-orbitals of Ti. In both cases, the extra electron in the anion species occupies the π^* -orbitals of the C₂ dimers. The calculated Mulliken charges in the two clusters are shown in Table 2. As expected, the bonding in structure (a) is of slightly more covalent nature due to the better orbital overlap, while structure (b) is slightly more ionic. This is the reason that structure (a) is more energetically favorable than structure (b) (Figure 4). Although the calculated EAs of the two structures are both close to the 2.5 eV experimental value, the simulated DOS spectrum of structure (a) resembles the PES spectrum much better than that of (b), as shown in Figure 5. This suggests that the electronic structure is also very sensitive to the structure. The fact that the calculated EA and DOS of structure (a) are in excellent agreement with the experiment and the fact that structure (a) has a better calculated BE value than structure (b) provide conclusive evidence that the Ti₃C₈ magic cluster has *D*_{3h} symmetry with the 3 C₂ dimers in the same plane as the three Ti atoms (a, in Figure 4).

For Ti₄C₈, we considered three structures composed of 4 Ti atoms and 4 C₂ dimers. The third structure (not shown) with 4 C₂ side-bonded to the four apexes of a tetrahedral Ti₄ cluster is 12 eV less stable than structure (a) in Figure 4 and can be easily eliminated. The lowest energy structure we found (a, Figure 4) involves 4 C₂ bonded at the 4 faces of the tetrahedral Ti₄ cluster. Structure (b) with 4 C₂ dimers bridging the four sides

**Figure 6.** Comparison of the photoelectron spectrum of Ti₄C₈⁻ to the calculated DOS of the two structures shown in Figure 4. See Figure 5 caption.**Table 3.** Calculated Mulliken Charges on the Four C₂ Dimers and the Ti Atoms in Ti₄C₈

structure	C ₂ dimer	Ti
a	-0.744	+0.744
b	-0.770	+0.770

of a square Ti₄ has a BE about 2.67 eV less favorable compared to structure (a). Furthermore, the calculated EA of structure (b) is also much smaller than the measured value of 1.8 eV. The EA calculated for structure (a) agrees well with the experimental value. In particular, the DOS of structure (a) fits the PES spectrum remarkably well, as shown in Figure 6. Therefore, we are confident that the structure of Ti₄C₈ is *D*_{2d} with 4 C₂ dimers bonded to the four faces of the tetrahedral Ti₄ (a, Figure 4). Interestingly, this structure can be considered to be derived by replacing the 4 corner C atoms of a 2 × 2 × 2 cubic Ti₄C₄ with 4 C₂ dimers. In this sense, Ti₄C₈ is rather similar to the cubic Ti₁₃C₂₂ cluster, which was derived by replacing the 8 corner C atoms of a 3 × 3 × 3 cubic Ti₁₃C₁₄ nanocrystal with 8 C₂ dimers (Figure 4).¹⁵ The structural similarity between Ti₄C₈ and Ti₁₃C₂₂ reinforces the prominent role of the C₂ dimers and the cubic framework in determining the structures of small titanium carbide clusters. Indeed, the driving force in the chemical bonding in Ti₄C₈ involves interactions between the π -orbitals of C₂ and the 3d-orbitals of Ti, similar to the situation in Ti₃C₈. However, the orbital mixing is much enhanced in Ti₄C₈ and this can be seen clearly from the enhanced Mulliken charges on the C₂ dimers, as shown in Table 3.

The mass spectrum shown in Figure 1 suggests that the growth from the 7/13 to the 13/22 cluster is rather rapid, resulting in very low abundance for clusters containing 8 to 12 Ti atoms. The prominent abundance of the 9/15 cluster in this size range indicates that it is particularly stable and may be an intermediate step along the growth path to Ti₁₃C₂₂. Therefore the structure of the Ti₉C₁₅ cluster may embody features of Ti₁₃C₂₂. As we pointed out previously in the layer-by-layer growth model, the 13/22 cluster can be viewed as a three-layer

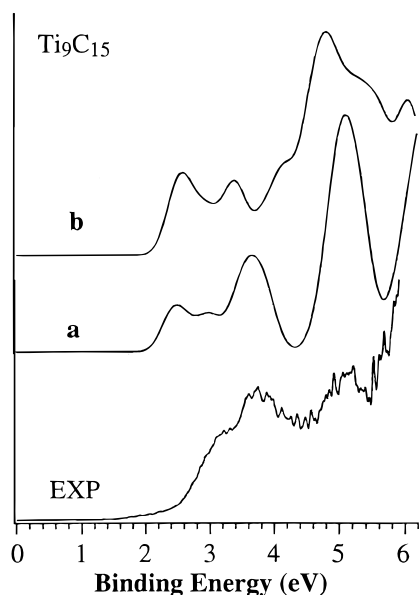


Figure 7. Comparison of the photoelectron spectrum of $Ti_9C_{15}^-$ to the calculated DOS of the two structures shown in Figure 4. See Figure 5 caption.

A–B–A structure (Figure 4), where A represents a Ti_4C_9 layer and B represents a Ti_5C_4 layer.¹⁵ A two-layer A–B structure would give a 9/13 cluster. Therefore, we considered the 9/15 cluster to be such a A–B structure with the two extra carbon atoms either being a C_2 dimer on top of the carbon-deficient B layer (**b**, Figure 4) or forming two additional C_2 dimers within the B layer (**a**, Figure 4). There are two possible positions for the C_2 dimer on top of the B layer, a symmetric and an asymmetric one (not shown), which are nearly degenerate. Structure (**a**) is the most strongly bound, and the calculated EA of this structure is also in excellent agreement with the measured value (Table 1). The simulated DOS spectra for structures (**a**) and (**b**) differ significantly: the one resulting from structure (**a**) resembles the PES spectrum better, as shown in Figure 7. Again, the consistent agreement between the calculated EA and DOS of structure (**a**) and the experiment supports this structure of Ti_9C_{15} .

We based the structures of both Ti_7C_{13} and Ti_6C_{13} on the two-layer Ti_9C_{13} cluster with incomplete B layers: Ti_7C_{13} and Ti_6C_{13} can be viewed as removing two and three Ti atoms from the complete Ti_5C_4 B layer, respectively. Two optimized structures were found for each cluster (Figure 4). Structure (**a**) in both cases is more favorable energetically and also gives EA values in much better agreement with the experiment (Table 1). The 4 C atoms in the partial B layer are rearranged to two C_2 dimers. The difference between the (**a**) and (**b**) structures in both Ti_7C_{13} and Ti_6C_{13} is that in the (**a**) structures the two C_2 dimers from the A layer are bonded to the two C_2 dimers in the partial B layer while in the (**b**) structures the two C_2 dimers from the A layer are flattened out without any bonding to the two C_2 dimers in the top layer. The calculated DOS spectra for the two isomers of Ti_7C_{13} and Ti_6C_{13} are compared to the PES spectra in Figures 8 and 9, respectively. Both the (**a**) and (**b**) structures of Ti_7C_{13} and Ti_6C_{13} yield relatively similar DOS spectra with that of the (**a**) structures in slightly better agreement with the PES spectra. While the calculated DOS curves for Ti_3C_8 and Ti_4C_8 give almost quantitative agreement with the experiment, the DOS curves of Ti_7C_{13} and Ti_6C_{13} can only be considered qualitatively. It is possible that in Ti_7C_{13} and Ti_6C_{13} both isomers might be present since their BE values only differ by about 1 eV and their overall structural features are quite

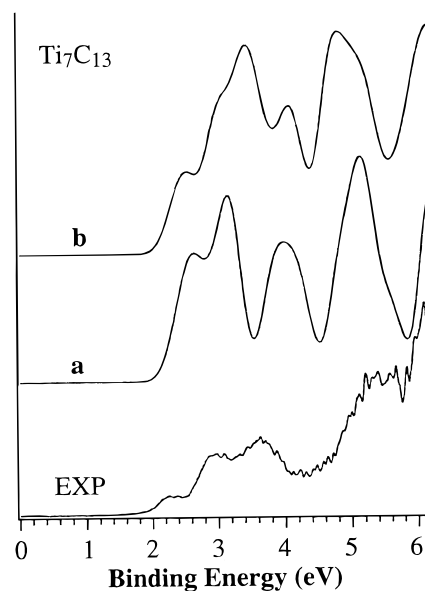


Figure 8. Comparison of the photoelectron spectrum of $Ti_7C_{13}^-$ to the calculated DOS of the two structures shown in Figure 4. See Figure 5 caption.

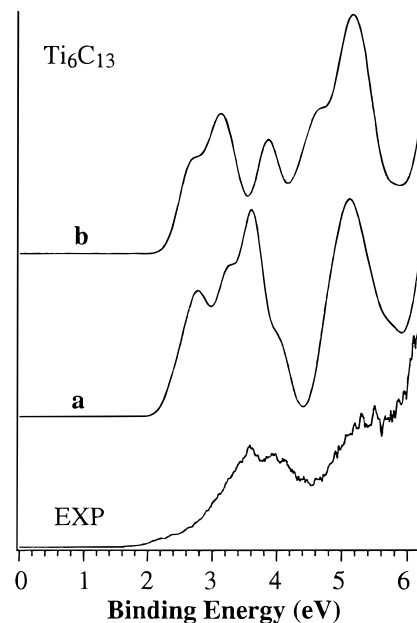


Figure 9. Comparison of the photoelectron spectrum of $Ti_6C_{13}^-$ to the calculated DOS of the two structures shown in Figure 4. See Figure 5 caption.

similar. However, the better agreement between the calculated EAs and DOS and the experiments does lend credence to structure (**a**) for Ti_7C_{13} and Ti_6C_{13} .

Growth Pathway to the Cubic $Ti_{13}C_{22}^-$ Cluster. On the basis of on our observed magic anion clusters and our insight into their structure and bonding, it would be interesting to speculate about the growth mechanisms of the carbide anion clusters and the formation of the cubic $Ti_{13}C_{22}^-$, since they may provide clues why MetCar was not formed in the anion channel. The structures of the magic clusters $Ti_3C_8^-$, $Ti_4C_8^-$, $Ti_6C_{13}^-$, $Ti_7C_{13}^-$, and $Ti_9C_{15}^-$ strengthen the importance of the cubic framework and the C_2 dimers in the growth of the $Ti_xC_y^-$ clusters and provide possible intermediates to the formation of the cubic $Ti_{13}C_{22}^-$. The mass distribution shown in Figure 1 is highly nonuniform with more abundant clusters always occurring around $Ti_6C_{13}^-/Ti_7C_{13}^-$ and $Ti_{13}C_{22}^-/Ti_{14}C_{24}^-$. We have

obtained similar mass patterns for a wide range of experimental conditions (0.1–5% CH₄ and different hydrocarbons CH₄/C₂H₂). There seem to be two rapid growth regions. The first one is from Ti₃C₈⁻ to Ti₆C₁₃⁻ and Ti₇C₁₃⁻, where the clusters between exhibit lower abundance. Many intermediate clusters are formed in this growth region with Ti₄C₈⁻ being more prominent. The second growth region is from Ti₇C₁₃⁻ to Ti₁₃C₂₂⁻. The growth in this region must proceed extremely fast since almost no intermediate clusters are survived except the Ti₉C₁₅⁻ cluster. The Ti₃C₈⁻ cluster, being the most prominent in the small size range, may be the key to set out the growth sequence. Therefore, Figure 4 from top to bottom probably represents the major growth steps leading to the formation of the Ti₁₃C₂₂⁻ cluster starting from Ti₃C₈⁻. The structural evolution of these clusters is highly systematic with the C₂ dimers, cubic framework, and layered structures being the essential components.

However, an important question still remains: why do the growth mechanisms seem so different between anions and cations in the titanium carbide system? We know that in the cation channels the dominating clusters are the MetCar Ti₈C₁₂⁺ and the cubic nanocrystal Ti₁₄C₁₃⁺. The Ti₁₃C₂₂⁺ cation has never been observed in the Ti_xC_y⁺ cluster system. We suspect that the presence of small C_n⁻ clusters, particularly C₂⁻, and the dominance of the Ti₃C₈⁻ cluster in the Ti/CH₄ plasma play the key role. The total absence of the MetCar Ti₈C₁₂⁻ anion in the Ti/CH₄ plasma system is another puzzling question despite our previous suggestion that the unusually low EA of Ti₈C₁₂ may be partially responsible.¹⁴ Answers to these questions will require systematic investigation of small carbide clusters (both anions and cations) from all the MetCar-forming early transition metal carbide systems, which we are actively pursuing.²²

Conclusions

We report new prominent clusters in the anion mass spectra of titanium carbide clusters, Ti_xC_y⁻, where $x/y = 3/8, 4/8, 6/13, 7/13, 9/15,$ and $13/22$, that do not exist in the positive ion mass spectra. Two growth regions were observed in the Ti_xC_y⁻ clusters from Ti₃C₈⁻ to Ti₆C₁₃⁻ and Ti₇C₁₃⁻ and from Ti₇C₁₃⁻ to Ti₁₃C₂₂⁻, where clusters between the two regions have low abundance. A combined photoelectron spectroscopy and density

functional theoretical study was carried out to understand the structure and bonding of these clusters and obtain insight into their growth pathways. All Ti_xC_y clusters were found to be primarily composed of three major components: C₂ dimers, cubic framework (except Ti₃C₈), and layered structures. Substantial charge transfer was found from Ti to C₂, and consequently C₂ in the Ti_xC_y clusters can be viewed as acetylene-like C₂ anions. The favorable orbital overlaps between the π -orbitals of C₂ and the d-orbitals of Ti give rise to strong bonding in the Ti_xC_y clusters. The calculated EAs and the simulated DOS spectra for all the clusters are in excellent agreement with the experimental measurements, lending considerable credence to the validity of the optimized cluster structures. It is remarkable that very moderate variations in the cluster geometries among the different isomers result in significantly different features in the DOS spectra and EA values and the lowest energy structures in all cases give the best agreement with experiments. The Ti₁₃C₂₂ cluster was previously proposed to have a novel cubic structure with 8 C₂ dimers replacing the 8 C atoms in a $3 \times 3 \times 3$ Ti₁₃C₁₄ cube. We found currently that Ti₄C₈ has a D_{2d} structure which can be viewed as replacing the 4 C atoms in a $2 \times 2 \times 2$ Ti₄C₄ cube with 4 C₂ dimers, a smaller version of the Ti₁₃C₂₂ cluster. A growth sequence is proposed starting from Ti₃C₈⁻ to Ti₁₃C₂₂⁻ with prominent intermediates at Ti₄C₈⁻, Ti₆C₁₃⁻, Ti₇C₁₃⁻, and Ti₉C₁₅⁻. The presence of small C_n⁻ clusters and the dominant Ti₃C₈⁻ cluster are suggested to play key roles in the growth of the Ti_xC_y⁻ clusters.

Acknowledgment. The support of this research by the National Science Foundation through a CAREER Program Award (DMR-9622733) is gratefully acknowledged. The experimental work was performed at Pacific Northwest National Laboratory, operated for the U.S. Department of Energy by Battelle under contract DE-AC06-76RLO 1830. The theoretical work was conducted at Air Products and Chemicals, Inc. H.C. gratefully acknowledges Drs. C. A. Valenzuela and J. B. Pfeiffer for support of this collaborative research.

JA9741990